Electronic Supplementary Material (ESI) for Biomaterials Science.

Supporting Information

Three-Dimensional Multilayered Fibrous Constructs for Wound Healing Applications

Tiago C. Reis,[a,b] Steven Castleberry,[b] Ana M. B. Rego,[c] Ana Aguiar-Ricardo*[a] and Paula T. Hammond*[b]

[a]LAQV-REQUIMTE, Departamento de Química, Faculdade de Ciências e Tecnologia, Universidade NOVA de Lisboa, 2829-516 Caparica, Portugal E-mail: air@fct.unl.pt

[b]Department of Chemical Engineering, Massachusetts Institute of Technology, 77 Massachusetts Avenue, Cambridge, MA 02139, USA. E-mail: hammond@mit.edu

[c]CQFM and IN, Instituto Superior Técnico, Universidade de Lisboa, 1049-001 Lisboa, Portugal.

Detailed Experimental Section

Constructs chemical characterization – Sample preparation and analysis: 10 mg of untreated and treated 3DECs were solubilized in $CDCl_3$ (99.8%, Cambridge Isotope Laboratories). ^{1}H-NMR spectra of each construct was obtained recording 96 scans per sample (ARX 400 MHz, Bruker). In parallel, portions from the top and bottom sides were delaminated and separately milled in KBr (1:200 w/w) being posteriorly pressed to form a disk. For each sample, a FTIR spectrum was recorded at a resolution of 1 cm^{-1} with a total of 128 scans (Spectrum 1000, Perkin Elmer). The constructs surface chemical composition was studied by X-ray Photoelectron Spectroscopy (XPS) and static contact angles. For the XPS analysis, as-spun and plasma treated electrospun constructs were cut in square sections (1×1 cm^2) and fixed to a holder by a metallic spring. Unmonochromatic Al Kα radiation (hυ = 1486.6 eV), from a spectrometer XSAM800 (Kratos Analytical) operated in a fixed analyzer transmission mode, was used. The operation parameters and data treatment methodology was followed as described elsewhere.[1] Charge accumulation was not compensated by a flood gun. The charge shift of the untreated and treated 3DECs was corrected setting the binding energy of the C 1s photoelectrons ejected from carbon in C-C and C-H bonds to 285.0 eV.[2] The following sensitivity factors were considered for quantification purposes: 0.25 (C 1s) and 0.66 (O 1s). Static contact angles (N=4) were measured at room temperature by applying the sessile drop method (CAM 100, KSV Goniometer). A 10 μL glycerol (≥99.0%, Sigma-Aldrich) drop was placed on the 3DECs surfaces (top and bottom). The acquisition time was extended up to 5 minutes with a frame interval of 300 ms. Each frame was retrieved to MatLab R2012b (MathWorks) and the drop height and base diameter were measured.

Hyaluronic acid fluorescence dye synthesis: HA fluorescence dye was synthesized for confocal microscopy use and release studies. 120 mg of HA were mixed with 50 mg of *N*–(3–dimethylaminopropyl)–*N*'–ethylcarbodiimide hydrochloride (EDC, ≥98%, Sigma-Aldrich) and 30 mg

of N–hydroxysulfosuccinimide sodium salt (NHSS, ≥98%, Sigma-Aldrich) in sodium acetate buffer (pH=5.0, 0.1 M) for 45 minutes. 60 mg of hexamethylenediamine (98%, Sigma-Aldrich) were posteriorly added and allowed to react during 4 hours, followed by three precipitation cycles in isopropanol to remove unreacted diamine. The hyaluronic acid amine derivative was then mixed with 0.5 mg of fluorescein isothiocyanate isomer I (FITC, ≥90%, Sigma-Aldrich) in a sodium bicarbonate solution (pH=8.5) during 8 hours in the dark. FITC-HA was then recovery by precipitation cycles in ethanol and two precipitation cycles in a mixture of ethanol/water. The absorbance of the supernatant was compared with a fresh mixture of ethanol/water, in order to conclude that non-reacted FITC was completely removed.

Table S1 Specifications of an ideal wound dressing[3, 4] and advantages in the use of poly(ε-caprolactone).

Characteristics	**Poly(ε-caprolactone)**
Non-toxic and non-allergenic	Biocompatibility[5]
Can be removed without causing trauma to the wound	Hydrophobic polymer (Reduces cell adherence). When placed onto the wound site, a layer of water molecules adheres to the biomaterial surface preceding the rapid attatchment of proteins. Cell adherence is then promoted in biointegrative manner, leading to tissue adhesion. By reducing the initial protein adsoption, wound dressings cause less trauma when removed.[6]
Impermeable to external microorganisms and fluids	Hydrophobic polymer (Protective external barrier)
Thermally insulating	Easily processed through different technologies allowing a deep control of the dressings inner structure (e.g. particulate leaching, thermaly induced phase separation, electrospinning, 3D printing, stereolitography, etc.)
Allows gaseous exchanges	
Reduced number of changes	Mechanical and Physicochemical stability in physiological medium[7]
Cost-effective	Low cost
Long shelf-life	Mechanical and Physicochemical stability[5]

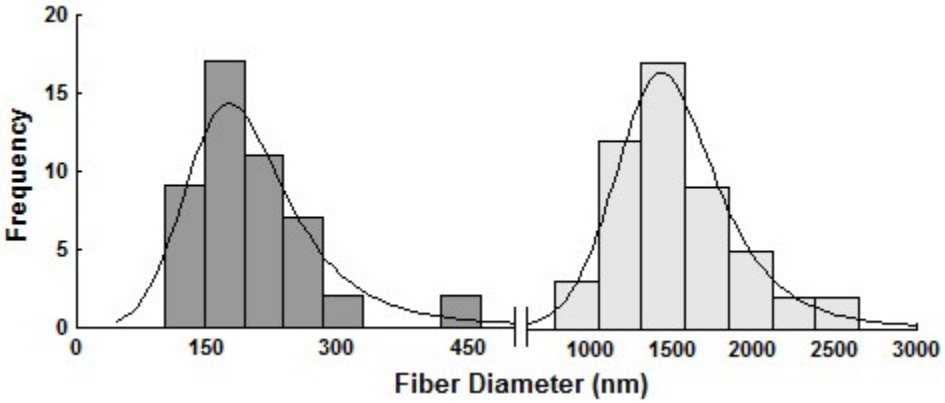

No. of populations identified	Distribution fitted	Distribution Parameters	Mean ± Std (nm)
2	1st, Log-logistic	a= 5.2631 ; b= 0.2143	208.4 ± 89.57
	2nd, Log-logistic	a= 7.3089 ; b= 0.1400	1542.8 ± 407.79

Fig. S1 3DECs fiber diameter distribution in the bottom side. The constructs shown a bimodal fiber distribution characterized by two independent log-logistic distribution (Population 1, BIC = 742.075; Population 2, BIC = 583.582).

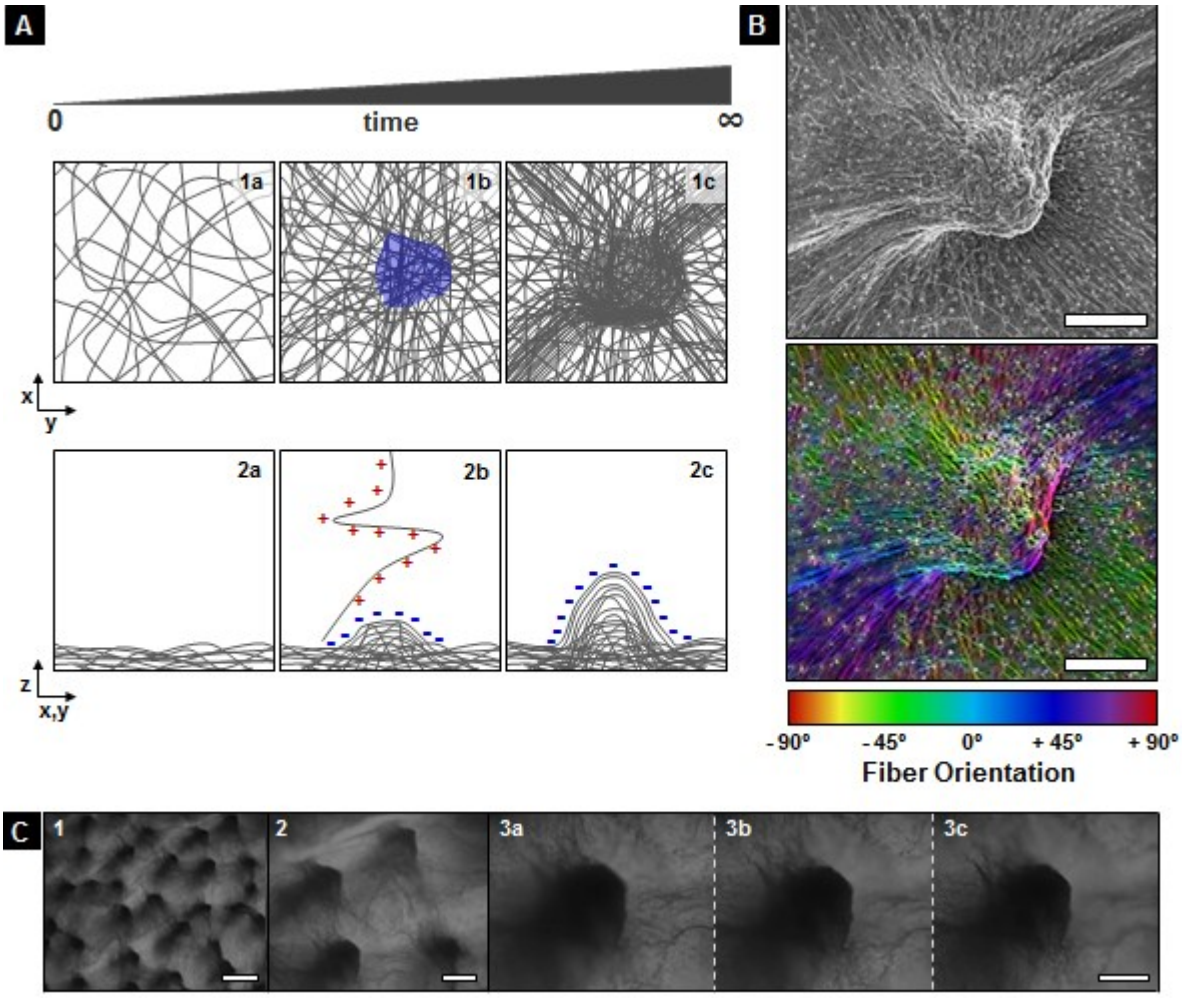

Fig. S2 Fibers self-assembly induced by their *in situ* polarization leads to the generation of protrusions. **A**, Scheme of the protrusions formation due to the fibers *in situ* polarization. As time passes by, the electrospun fibers acquire a negative superficial charge that drives the incoming aerial positive fibers to be collected on top of them. The electrostatic forces of attraction generate a densely packed fibrous network, shaping tightly the self-assembled construct into protrusions. **B**, SEM micrographs and fiber colored orientation analysis (scale bar = 100 μm). **C**, DIC microscopy images from the top side evidencing multiple protrusions with a conical shape. (Image 1, scale bar = 500 μm; image 2, scale bar = 200 μm; image 3a-3c, scale bar = 50 μm). Images 3a-3c were taken at different z-planes.

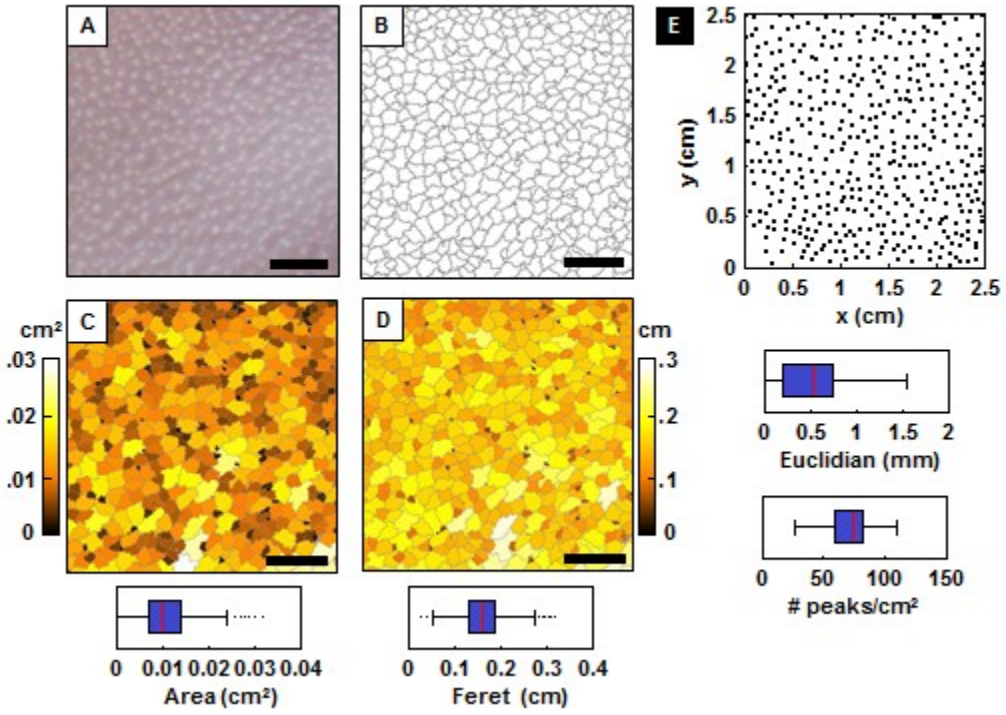

Fig. S3 3DEC topographic characterization. **A**, 3DEC top side photograph evidencing protrusions. **B**, Image optimal segmentation by cell elements. **C**, Cell area distribution. **D**, Cell Feret diameter distribution (A-D images, scale bar = 500 mm). **E**, Scattered protrusions centroids with determination of the interprotrusion Euclidian distance and protrusion density.

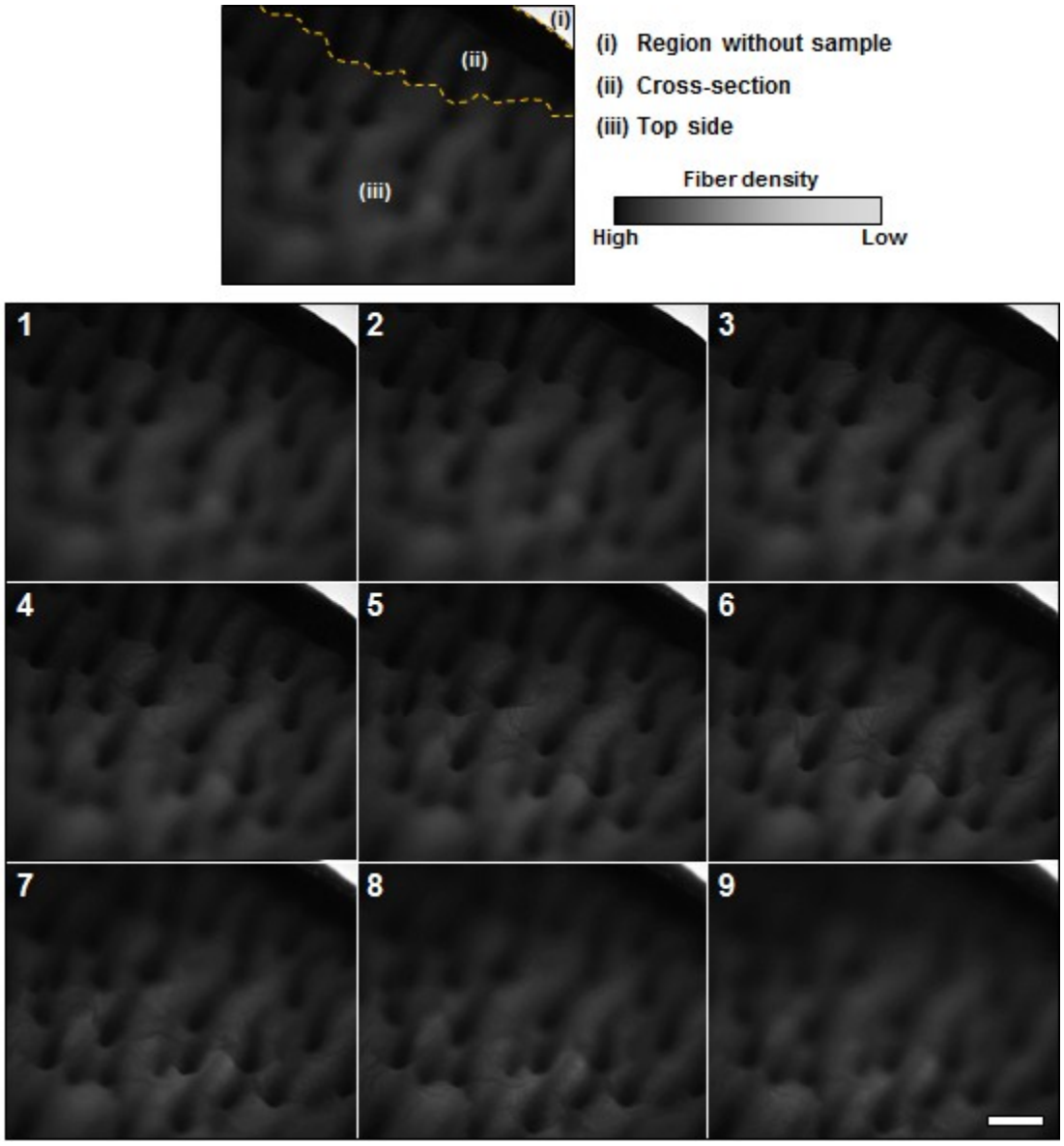

Fig. S4 Phase contrast microscopy images from a 3DEC, including the cross-section and top side at different z-planes, evidencing, simultaneously, multiple protrusions and z-axis built in core characterized by dense fiber regions (scale bar = 500 μm).

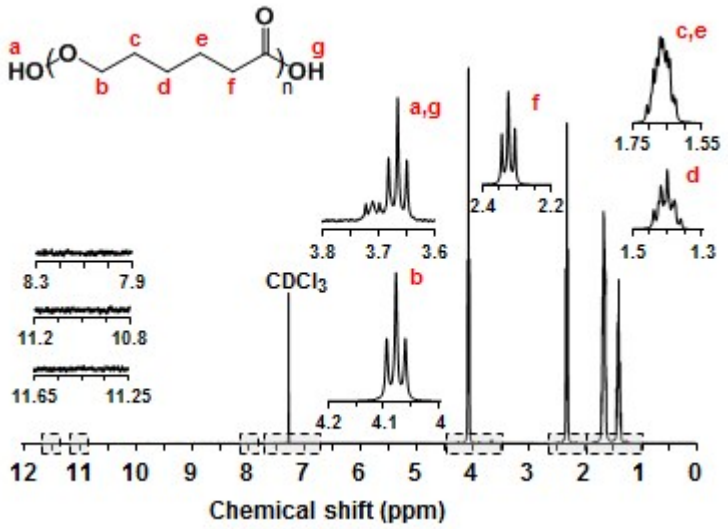

Fig. S5 Solvent contamination assessment by ^{1}H NMR of as-spun 3DECs in $CDCl_3$. In case of contamination shifts at 2.10 and 11.40 ppm (acetic acid) and/or 2.10 and 8.27 ppm (formic acid) should be noticed.[8]

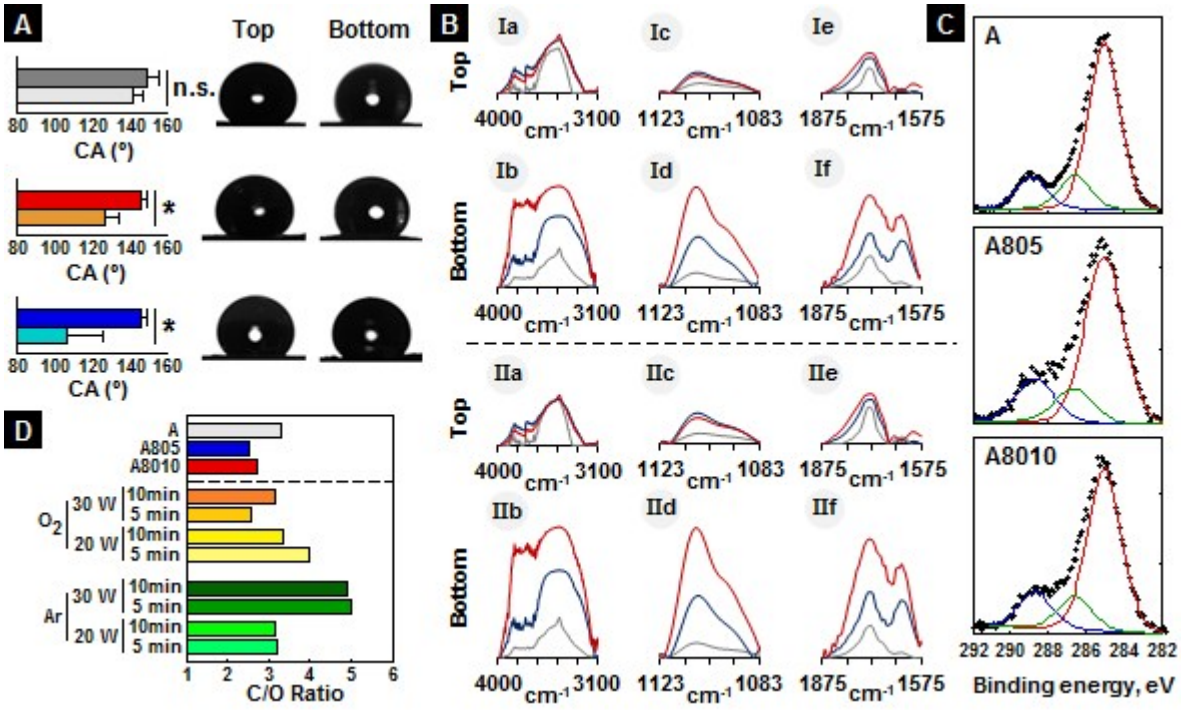

Fig. S6 3DECs chemical characterization after plasma treatment. **A**, Static contact angle determination (n.s., not significant; *, p-value < 0.01). **B**, FTIR spectra at different sides (A, grey; A5, blue; A10, red) normalized by $\upsilon_{S(CH2)}$ (Ia-f) and $\upsilon_{AS(CH2)}$ (IIa-f) in the following characteristic bands: $\upsilon_{(OH)}$, 3000-4000 cm^{-1}; $\upsilon_{(C=O)}$, 1729 cm^{-1}; $\upsilon_{(C-O)}$, 1108 cm^{-1}. **C,** XPS spectra of high resolution C 1s core level signal (Blue, Ester functional groups, O–C=O, and/or carboxylate functional groups, O-C=O^{-}; Green, Carbon singly bound to oxygen –C–OH or –C–O–; Red, Aliphatic carbon in bonds –C–C– or –C–H). **D,** Carbon/Oxygen ratio determination from elemental surface composition (A, C

1s: 76.6 & O 1s: 23.4; A5, C 1s: 71.3 & O 1s: 28.7; A10, C 1s: 72.9 & O 1s: 27.1). Data comparison with similar reported plasma treatment strategies of 2D non-woven PCL meshes.[9]

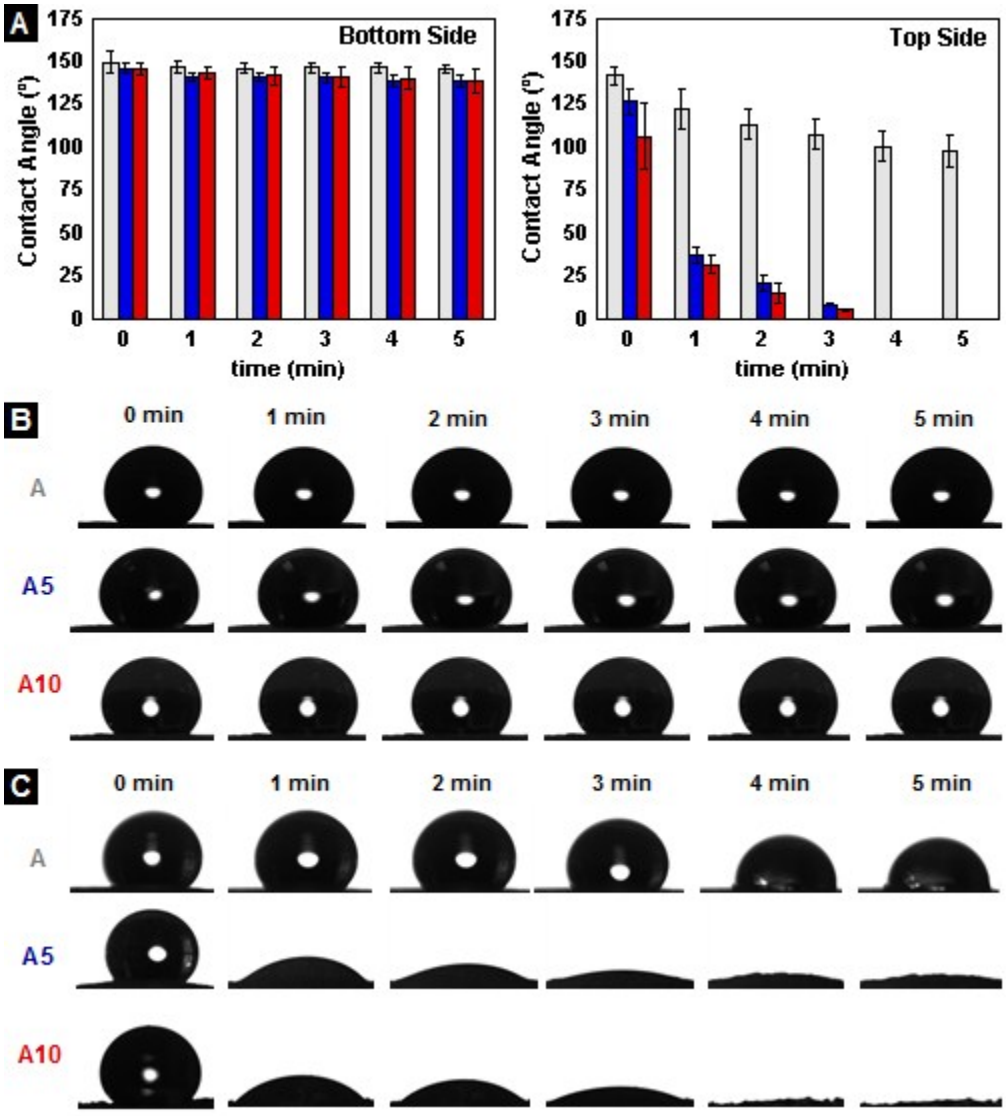

Fig. S7 Spreading and imbibition dynamics. Extended contact angle measurements (**A**) and corresponding images from the bottom (**B**) and top (**C**).

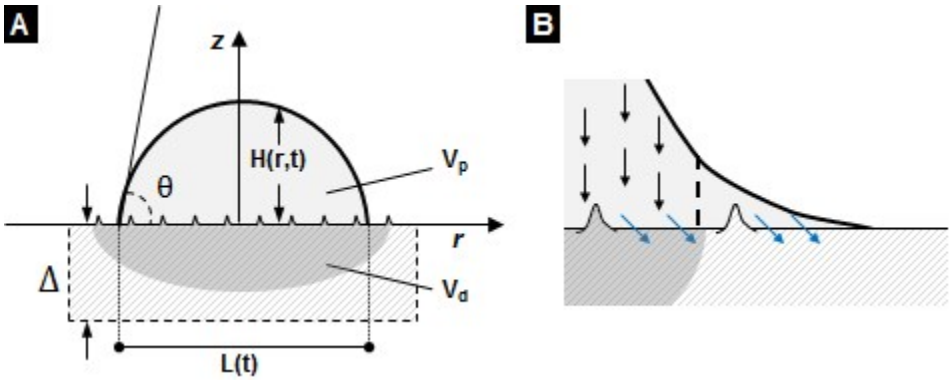

Scheme S1 Resting droplet assay in a 3DEC construct. **A**, Spreading and imbibition study variables: Δ, construct thickness; θ, contact angle; H, drop height; L, drop base diameter; V_p, droplet volume; V_d, imbibed droplet volume; **B**, Oblique liquid absorption as a combination of the spreading and imbibition stages (blue arrows).

As previously highlighted, an ideal dressing is described as a construct which is impermeable to external liquids (avoiding sources of infection), while still allows the wound exudate uptake at the dressing-tissue boundary. The kinetics of wound exudate absorption over a porous wound dressing results of an interplay of two processes: i) the exudate spreading on the dressing interface, and ii) the exudate imbibition into the dressing inner structure. The superposition of the spreading and imbibition stages can be described as:

$$\frac{dH}{dt} = u^* + u^0 \qquad (S1)$$

where *H* is the height of a resting test drop in the material surface, u^* and u^0 are the velocities of the spreading and imbibition stages. It is important to note that the free energy (Φ) of a fluid drop with a volume *V*, in contact with a 3DEC surface, can be described as:

$$\phi = \gamma S + P_e V + \pi\left(\frac{L}{2}\right)^2\left(\gamma_{SL} - \gamma_{SV}\right) \qquad (S2)$$

where γ is the liquid surface tension, *S* is the liquid-air interface area, P_e is the excess pressure inside the droplet, γ_{SL} and γ_{SV} are the solid-liquid and solid-vapor interfacial tension respectively. According to the previous equation, the free energy of a liquid drop is proportional to the dressing-liquid interfacial tension and it is also proportional to the square of the drop base diameter (L). As shown in Figure 1, the induced z-axis asymmetric fiber deposition in 3DECs favors the formation of a protective fibrous bottom layer due to a higher fiber density in this side. Therefore, the produced 3DECs have a pore size and hydrophobic gradient across the constructs' thickness, favoring the presence of side dependent fluid handling properties in the same material. Analogous to Martins et al.,[9] the contact angle measurements relied on the use of glycerol due to the similarity of its surface tension ($\gamma_{25°C}$=62.4 mN.m^{-1}) with the water surface tension ($\gamma_{25°C}$=72.0 mN.m^{-1}) and the viscous-like behavior comparatively to wound exudate. From **Fig. S7**, one can observe that the contact angle at the 3DECs bottom side does not change regardless the time or type of construct. This observation

is aligned with our earlier findings. Previously we showed that despite the use of plasma to chemically modify 3DECs, the use of a metallic plate hindered the functionalization in this region, contributing to a chemically unmodified bottom side. Therefore, A5 and A10 evidence a similar chemical composition comparatively to A at this region, leading to similar γ_{SL} and γ_{SV} values in this construct's side. In addition, it was also possible to observe earlier that the bottom side fibrous network is structurally similar in A, A5 and A10, which contributes to comparable solid-liquid interfaces. Hence, according to equation S2, and since the characterization approach was the same for all the specimens, $\Phi_A \sim \Phi_{A5} \sim \Phi_{A10}$ in this region of the dressings, justifying the similar contact angles observed at this constructs side. Moreover, at this 3DECs side, the drop spreading and imbibition do not take place, leading to an unperturbed droplet base radius and profile. As stated above, the first stage of a drop motion in contact with a dressing is the spreading, meaning the motion of the three-phase contact line through the dressing surface (**Scheme S1**). Such motion results from the *in situ* distortion of the droplet spherical shape caused by its capillary pressure (P_{cap}), generating a new incremental contact region where the disjoining pressure (Π) comes into play.[10] If $\Pi < P_{cap}$, the liquid in contact with the wound dressings spreads, otherwise if $\Pi > P_{cap}$ the spreading does not occur which is observed in the constructs top side. According to the DLVO theory, the total disjoining pressure is a sum of two main components: molecular (Π_m) and electrostatic (Π_e), where $\Pi(H) \sim \Pi_m(H) + \Pi_e(H)$. The molecular component of the disjoining pressure results from the van der Waals forces acting at the interfacial region,[11] while the electrostatic component results from the electrostatic interaction between the surface and contacting liquid. Moreover, the total disjoining pressure is proportional to the Gibbs free energy per unit of the interlayer area,[12] meaning that favorable dispersive and electrostatic forces, between the dressing and the contacting liquid, promote the droplet initial spreading (lower values of Π). In the case of the 3DECs bottom side, the differences in the polarity of the non-functionalized PCL fibers and glycerol hindered their intermolecular interactions, contributing for a higher disjoining pressure in comparison to the droplet capillary pressure, which inhibits the liquid spreading and imbibition at the 3DECs bottom side. Due to the z-axis asymmetric fiber deposition, the 3DECs topography at their top side is microtexturized. The observed higher hydrophilic functionalization, offer a distinct environment for liquid spreading and imbibition. According to Fig. S9, it is possible to observe the contact angle decay in all the tested specimens, where the A type constructs evidence the highest contact angle measurements. Furthermore, it is also possible to verify a distinct drop profile and dynamic base diameter in all the analyzed constructs comparatively to the 3DECs top side. As stated above, the first stage in a droplet motion is the droplet's spreading. If this stage is hindered, the imbibition of the contacting liquid is compromised. In this way, in order to enhance the wound exudate uptake process, the wound dressing must initially favor the condition $\Pi < P_{cap}$, by tuning the chemical nature of the dressing while aiming to enhance the intermolecular interaction with the wound exudate. The top surface functionalization of the dressings A5 and A10, in comparison with the A type constructs, enhances the spreading stage where u^* is 1 order of magnitude faster. In

addition, these plasma treated 3DECs showed a total liquid imbibition at t ~ 3 minutes, while the A type dressings present an extrapolated time value of ~ 14 minutes for total imbibition as well. While the bottom side of the produced 3DECs are structurally and chemically similar, their top sides only resemble in their structure, leading to different spreading and imbibition dynamics. Despite the chemical surface modification, the topography of the 3DECs top side reveals to be also important. When comparing the top and bottom sides of the A type wound dressings, which have the same chemical composition, it is possible to observe a distinct drop spreading and imbibition at the top side. According to Darcy's equation, the liquid imbibition over a saturated dressing can be described as:

$$\frac{dH}{dt} \sim \frac{K_p}{\eta} * \frac{P_{cap}}{z} \qquad (S3)$$

where $-\Delta<z<0$ and K_p is the permeability of the porous dressing. Several authors[13] have successfully correlated K_p with the porosity of fibrous materials. Generally, it is observed that as the materials' porosity increases the construct becomes more permeable, since the resistance of the porous medium to flow decreases. Thus, the observed pore size gradient across the membranes thickness favors the wound exudate transport at the top side towards the construct bottom side, while simultaneously hinders the imbibition of external contaminated liquids on the opposite direction.

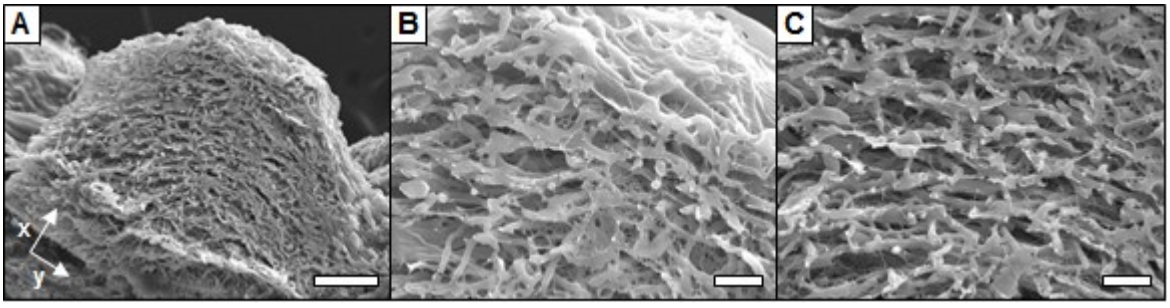

Fig. S8 SEM cross-section images of a coated protrusion evidencing the electrospun fibers self-assembly. The fiber based network evidences a high tortuosity. (A, scale bar = 50 μm; B/C, scale bar = 10 μm).

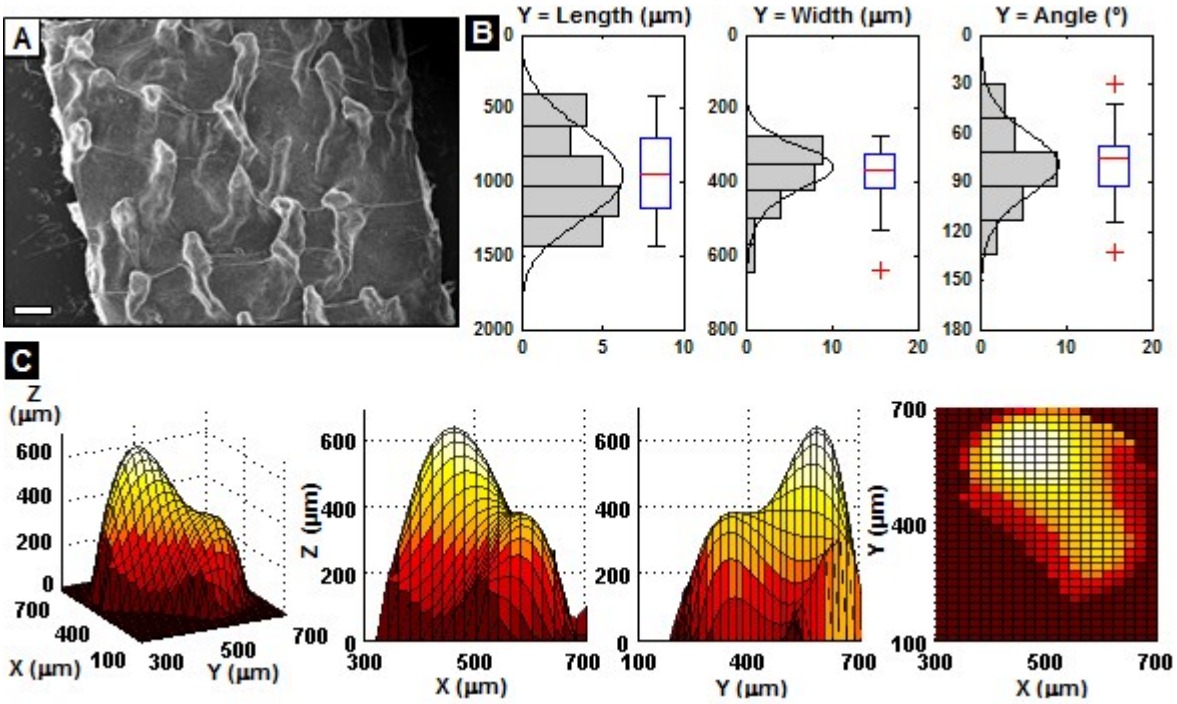

Fig. S9 LbL coated protrusions characterization. **A**, SEM image from a 3DMEC top side (scale bar = 500 µm). **B**, Shape descriptors distributions. **C**, Three-dimensional reconstruction of a coated protrusion.

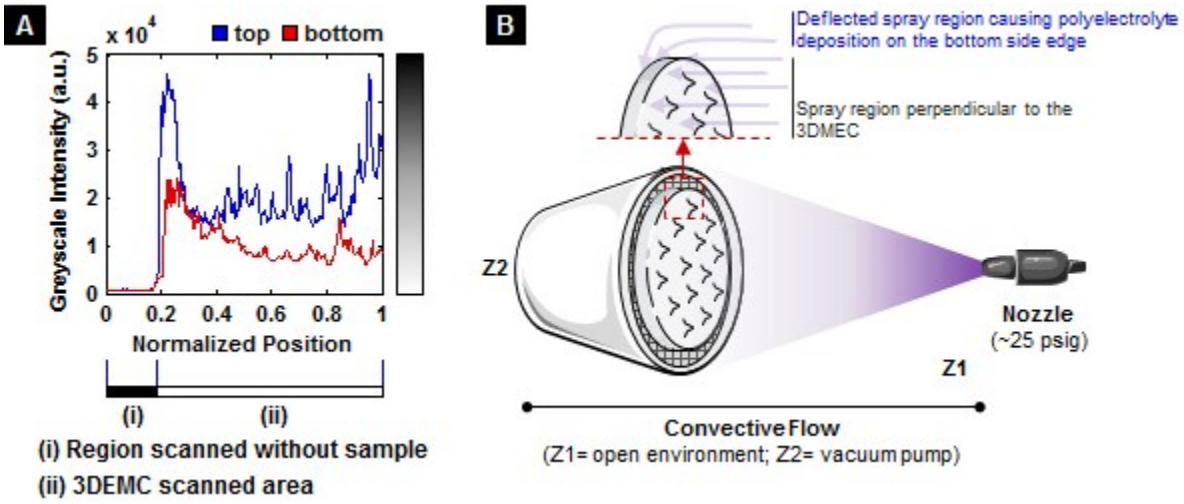

Fig. S10 **A**, $(CHI/FITC\text{-}HA)_{10}$ film deposition assessment on three-dimensional multilayered electrospun constructs according to their side. **B**, 3DMEC fixation scheme in the spray-LbL process, illustrating sprayed-polyelectrolyte flow and edge crossover.

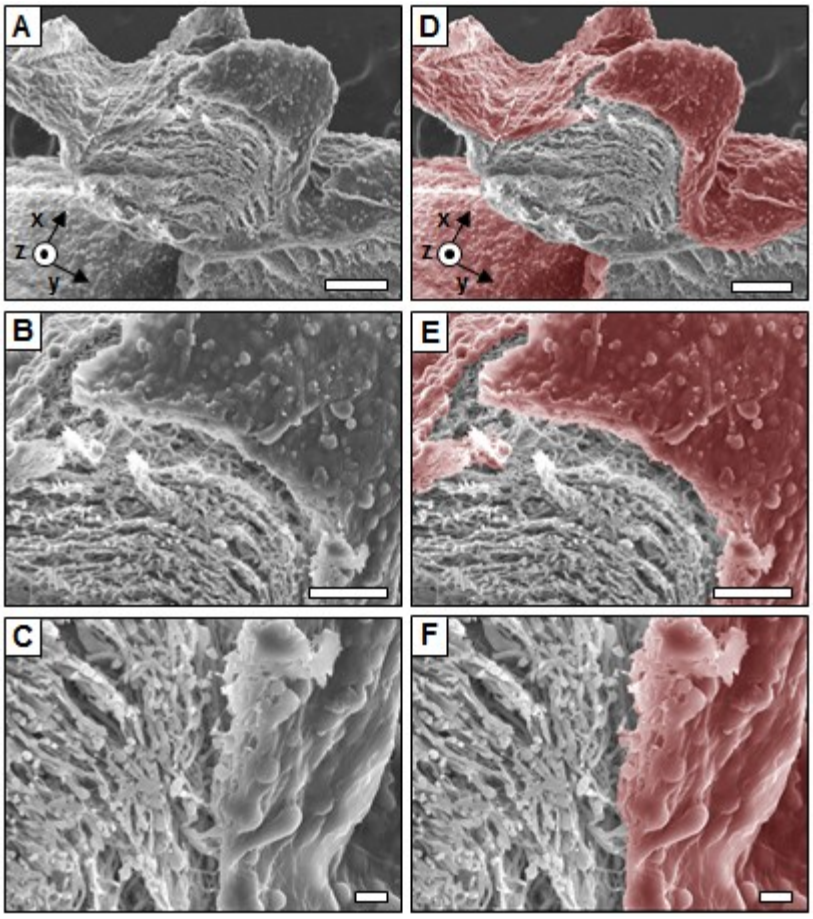

Fig. S11 SEM images (A, B and C) and pseudo-colored SEM (D, E and G) of a pulled out coated protrusion. (A/D, scale bar = 100 μm; B/E, scale bar = 50 μm; C/F, scale bar = 1 μm).

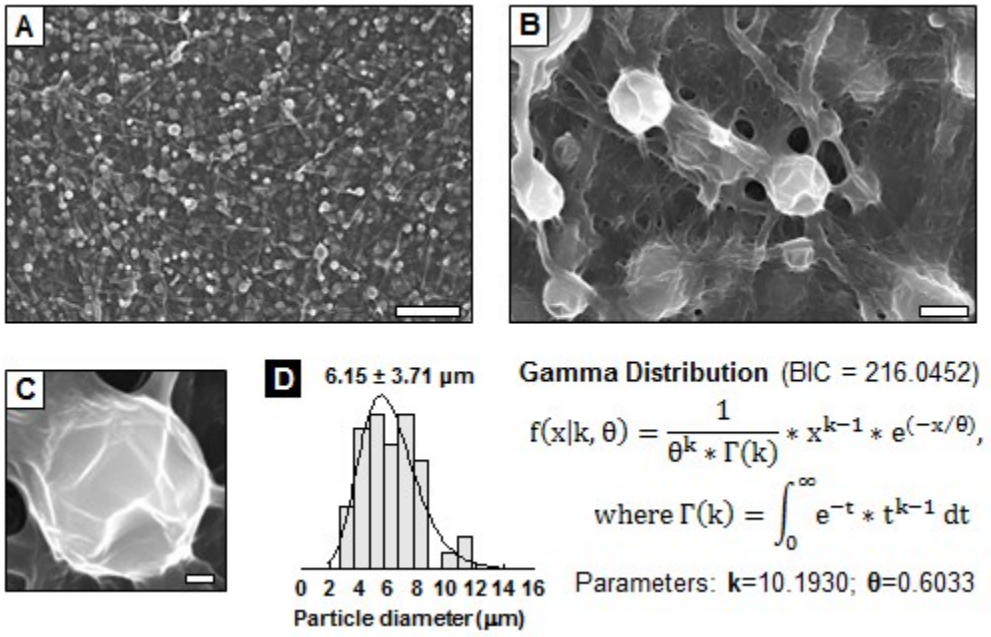

Fig. S12 Morphological characterization at the interprotrusion space. SEM images at different magnifications (**A**, scale bar = 50 µm; **B**, scale bar = 5 µm; **C**, scale bar = 1 µm). **D**, Microparticle distribution (N=50; BIC, Bayesian Information Criteria).

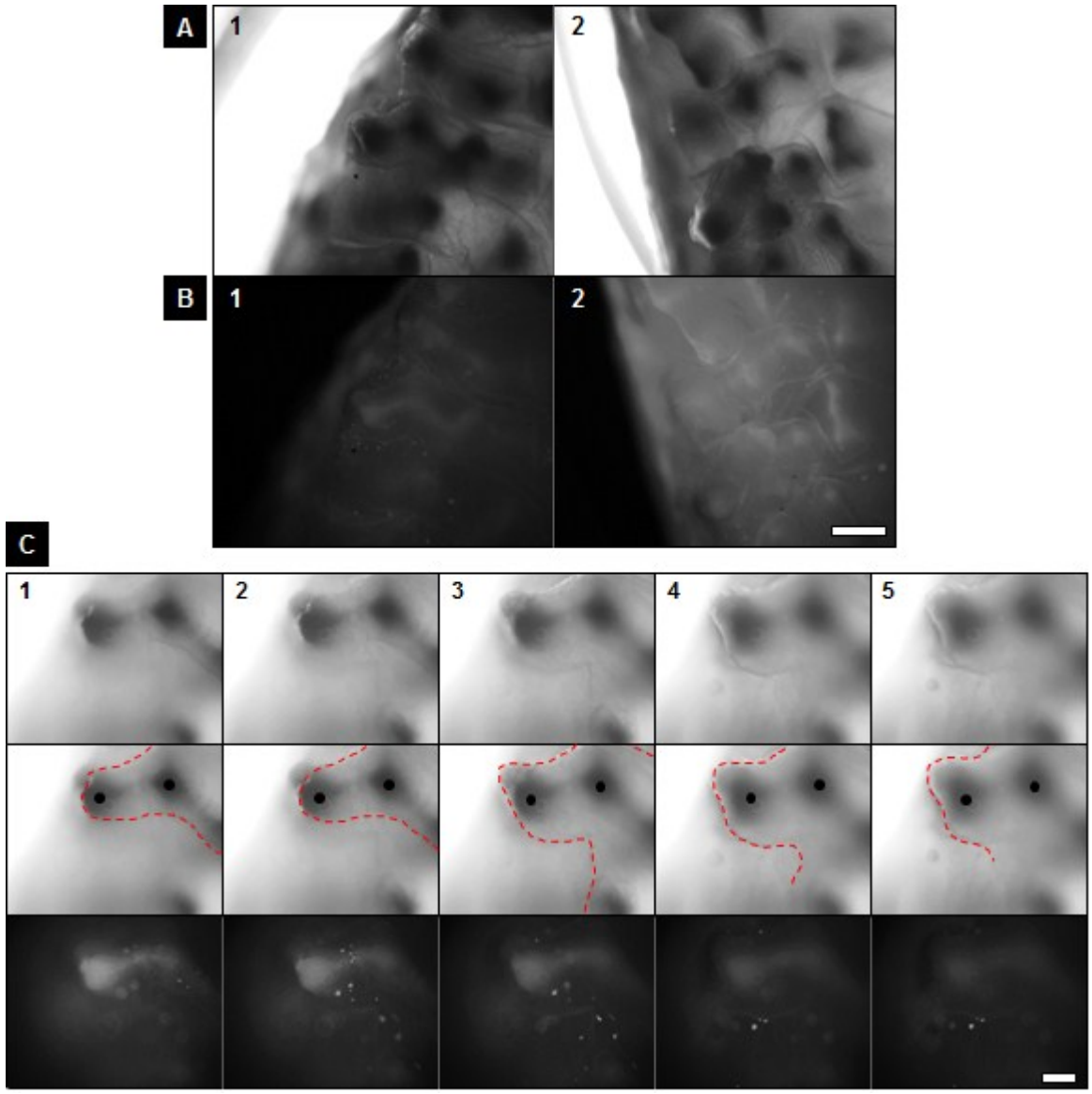

Fig. S13 Phase contrast and fluorescent microscopy images of cell seeded 3DMECs top side evidencing the LbL film swelling (**A**,**B** scale bar = 500 μm; **C**, scale bar = 200 μm). Dark dots were placed at the protrusions center.

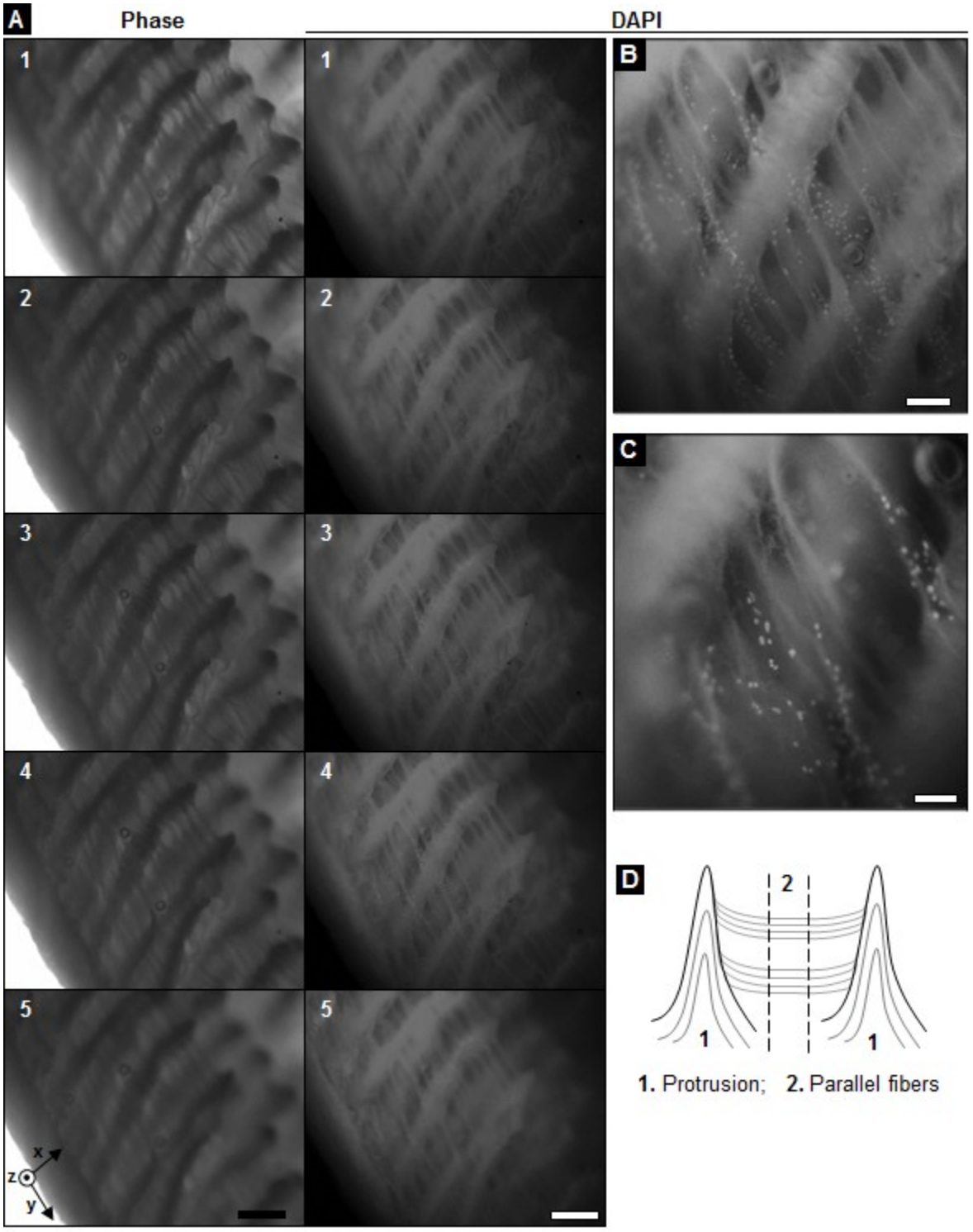

Fig. S14 Phase contrast and fluorescent microscopy images from a cell seeded 3DEC top side at different z-planes evidencing simultaneously multiple protrusion, z-axis built in formation and parallel fibers between protrusions (**A**, scale bar = 500 µm; **B**, scale bar = 200 µm; **C**, scale bar = 100 µm). **D**, Scheme regarding the presence of parallel fibers between protrusions.

Table S2 Protrusion features distributions.

Characteristic	Distribution fitted	Distribution Parameters	Mean ± Std
Length	Weibull (BIC: 332.908)	a= 1048.4 ; b= 3.6429	945.3 ± 288.56 (μm)
Width	Log-logistic (BIC: 270.867)	a= 5.9064 ; b= 0.1136	375.3 ± 79.36 (μm)
Angle	Inverse Gaussian (BIC: 503.526)	μ= 162.8800 ; λ= 3403.6	81.9 ± 27.83 (º)

Weibull Distribution

$$f(x \mid a,b) = \frac{b}{a} * \left(\frac{x}{a}\right)^{b-1} * \exp\left(-\frac{x}{a}\right)^{b}, \quad for\ x \geq 0$$

Log-Logistic

$$f(x \mid a,b) = \frac{1}{b} * \frac{1}{x} * \frac{e^{z}}{(1+e^{z})^{2}}, \quad for\ x \geq 0 \quad and \quad where\ z = \frac{\log(x) - a}{b}$$

Inverse Gaussian Distribution

$$f(x \mid \mu,\lambda) = \sqrt{\frac{\lambda}{2\pi x^{3}}} * \exp\left[-\frac{\lambda(x-\mu)^{2}}{2\mu^{2}x}\right], \quad for\ x \geq 0$$

Birnbaum-Saunders Distribution

$$f(x \mid k,\theta) = \frac{1}{\sqrt{2\pi}} * \exp\left[-\frac{\left(\sqrt{x/a} - \sqrt{a/x}\right)^{2}}{2b^{2}}\right] * \left[\frac{\left(\sqrt{x/a} + \sqrt{a/x}\right)}{2bx}\right], \quad for\ x \geq 0$$

References

1. C. Nunes de Carvalho, G. Lavareda, P. Parreira, J. Valente, A. Amaral and A. M. Botelho do Rego, *J. Non-Cryst. Solids*, 2008, **354**, 1643-1647.
2. H. Hantsche, *Adv. Mater.*, 1993, **5**, 778-778.
3. T. Abdelrahman and H. Newton, *Surgery (Oxford)*, 2011, **29**, 491-495.
4. V. Jones, J. E. Grey and K. G. Harding, *Brit. Med. J.*, 2006, **332**, 777-780.
5. M. A. Woodruff and D. W. Hutmacher, *Prog. Polym. Sci.*, 2010, **35**, 1217-1256.
6. D. Farrar, *Advanced Wound Repair Therapies*, Elsevier Science, 2011.

7. C. X. F. Lam, D. W. Hutmacher, J. T. Schantz, M. A. Woodruff and S. H. Teoh, *J. Biomed. Mater. Res. A*, 2009, **90A**, 906-919.
8. W. M. Haynes, *CRC Handbook of Chemistry and Physics, 93rd Edition*, Taylor & Francis, 2012.
9. A. Martins, E. D. Pinho, S. Faria, I. Pashkuleva, A. P. Marques, R. L. Reis and N. M. Neves, *Small*, 2009, **5**, 1195-1206.
10. L. Boinovich and A. Emelyanenko, *Colloid Surface A*, 2011, **383**, 10-16.
11. L. Li, M. H. Kopf, S. V. Gurevich, R. Friedrich and L. Chi, *Small*, 2012, **8**, 487-503.
12. L. Boinovich, *Curr. Opin. Colloid. In.*, 2010, **15**, 297-302.
13. F. A. L. Dullien, *Porous media : fluid transport and pore structure / F. A. L. Dullien*, Academic Press, New York, 1979.